

Efficient two-mode interferometers with spinor Bose-Einstein condensates

Artur Niezgoda, Dariusz Kajtoch and Emilia Witkowska
Institute of Physics, PAS, Aleja Lotników 32/46, PL-02668 Warsaw, Poland
(Dated: September 9, 2019)

We consider general three-mode interferometers using a spin-1 atomic Bose-Einstein condensate with macroscopic magnetization. We show that these interferometers, combined with the measurement of the number of particles in each output port, provide an ultra-high phase sensitivity. We construct effective two-mode interferometers which involve two Zeeman modes showing that they also provide an ultra-high phase sensitivity but of a bit reduced factor in the corresponding Fisher information. A special case of zero magnetization is shown to persist the efficiency of the two-mode interferometry.

PACS numbers: 03.67.Bg, 03.75.Dg, 03.75.Gg.

I. INTRODUCTION

Spinor Bose-Einstein condensates proved to be an ideal candidate for high resolution sensitive magnetometers [1–7], where information about magnetic field strength is encoded in $2F + 1$ magnetic sublevels of the total spin F hyperfine manifold. Many theoretical proposals [8–13] as well as experiments [14–18] have demonstrated generation of highly entangled quantum states in spinor condensates, thus opening up the possibility for entanglement-enhanced atomic magnetometers operating below the standard quantum limit (SQL). Exceptional functionality of atomic sensors is based on the quantum interferometry techniques [19].

In the quantum interferometry scheme, a physical quantity like the magnetic field is mapped onto a phase difference θ between the internal states of the atoms, and can be estimated by performing number of quantum measurements at the output [20]. The most widely utilized technique is based on the measurement of a single observable that provides a well behaved monotonic signal as a function of θ . It may happen, that in order to fully exploit the potential of the system a knowledge of entire conditional probability distribution is necessary [21, 22]. Regardless of the estimation strategy, a precision in the θ estimation is bounded from below via the Cramér-Rao inequality $\Delta\theta \leq 1/\sqrt{\nu\mathcal{I}}$ [23], where ν is the total number of measurements and \mathcal{I} is the Fisher information (FI) [24] which depends on the input state, interferometric protocol and measurement. Clearly, modification of the measurement changes the estimation precision. According to the quantum Cramér-Rao theorem [25] the FI cannot be larger than the quantum Fisher Information F_Q (QFI), which is the maximized FI over all allowable quantum measurements. Substituting F_Q in place of \mathcal{I} in equation for $\Delta\theta$ yields the ultimate lower bound on the precision achievable by a quantum mechanical strategy. The scaling of the QFI with the total atom number N is of main interest. In the SQL $F_Q \propto N$ and is reached with uncorrelated atoms, while in the ultimate Heisenberg limit $F_Q \propto N^2$ (HL) and is possible when entangled states are used in the interferometry. In principle, the precision in the magnetic field sensing can be significantly increased

by employing entangled states in atomic magnetometers.

Here, we are interested in the interferometric utility of spin-1 Bose-Einstein condensates with three internal states numerated by the quantum magnetic number $m_F = 0, \pm 1$ for the situation of current experimental relevance [26], where the total number of atoms and the magnetization $M \equiv \langle \hat{J}_z \rangle = \langle \hat{N}_{m_F=1} \rangle - \langle \hat{N}_{m_F=-1} \rangle$ are both conserved. Additionally, the optical dipole trap is tight enough that the condensate forms in the single spatial mode with thermally populated internal degrees of freedom [27]. In [9], by calculating the QFI, we have shown that it is possible to overcome the SQL if the variance of magnetization ΔM is smaller than \sqrt{N} , and even approach the HL if $\Delta M < 1$ when using such thermal states. In this work we pursue further our study focusing on an optimal measurement which maximizes the FI and on an accessible with current experimental techniques interferometric transformations.

In the paper we concentrate on the measurement of the number of particles in each Zeeman component showing that it maximizes the FI for the most optimal three-mode interferometric transformations. Although, the three-mode interferometric transformations which optimally employ the QFI are not the representative ones, we show how they could be constructed in an experiment. We propose also to use a two-mode interferometric transformation equivalent to the Mach-Zehnder interferometer (MZI) in appropriate choice of the $SU(2)$ subspace. In practice, it means a reduction of the system to the two-mode description by truncation of the density matrix over unused by the interferometer third mode. Then, by using such two-mode interferometric transformations the HL is still possible to reach with slightly reduced factor in some cases only. We show also how to construct an effective two-mode interferometer for the system consisting of atoms having an arbitrary large value of the spin F . The conclusion is suitable for any value of magnetization, including the special case of widely studied zero magnetization. It is worth to notice that non-zero temperatures considered by us do not destroy the HL of the FI. Moreover, thermal fluctuations among internal degrees of freedom can be a resource for transition from the SQL to the HL in some cases.

In addition, we analyzed the estimation precision of effective two-mode interferometers using error-propagation formula and measurement of \hat{S}_z^2 or parity operator. In general, the quantum Cramér-Rao bound cannot be saturated in both cases, except $M = 0$ when \hat{S}_z^2 is optimal. However, in a special case when the third mode is completely depleted, the parity measurement is optimal for any value of magnetization.

Nonzero variance of magnetization, however has destructive impact on the precision in the θ estimation as we have already pointed out in [9]. When $\Delta M > 1$ then the measurement of populations of Zeeman components is not the most optimal one as the FI slightly differs in the value from the QFI. However, the measurement is not the worst option because the FI shows, similarly as the QFI, that the SQL can be still overcome if the variance of magnetization is smaller than \sqrt{N} .

II. STATE-OF-THE-ART

The system we focus on is a spin-1 atomic condensate in a homogeneous magnetic field [26, 28]. We assume the single mode approximation is valid [29–33]¹, and all atoms share the same spatial wave-function $\phi(\mathbf{r})$, which is a solution of the Gross-Pitaevskii equation with normalization $\int d^3r |\phi(\mathbf{r})|^2 = 1$ [34]. The many-body system Hamiltonian reduces to [9–11, 16, 35–38]

$$\frac{\hat{H}}{\tilde{c}} = \frac{\text{sign}(c_2)}{2N} \hat{J}^2 - q \hat{N}_0, \quad (1)$$

where \hat{J}^2 is the total spin operator and \hat{N}_{m_F} is the particle number operator for the Zeeman state $m_F = 0, \pm 1$. The energy unit is $\tilde{c} = N|c_2| \int d^3r |\phi(\mathbf{r})|^4$, where $c_2 = 4\pi\hbar^2(a_2 - a_0)/3\mu$, μ is an atomic mass, and a_0 and a_2 are the s-wave scattering lengths [32]. For $c_2 < 0$ (e.g. rubidium-87) the interaction term favors the ferromagnetic phase, with maximal total spin length $J = N$, whereas for $c_2 > 0$ (e.g. sodium-23) the antiferromagnetic phase minimizes the interaction energy with minimal spin length $J = 0$ [28]. The second term in (1) describes the quadratic Zeeman energy². The total number of atoms operator $\hat{N} = \sum_{m_F} \hat{N}_{m_F}$ and the z-component of

the collective spin operator $\hat{J}_z = \hat{N}_{+1} - \hat{N}_{-1}$ are both conserved. Terms proportional to \hat{N} and \hat{J}_z have no influence on the results, and they were dropped in the final form of (1). When the total number of atoms is fixed, the Hamiltonian (1) has a block-diagonal structure in the Fock state basis with each block labeled by the magnetization $M = -N, -N + 1, \dots, N$, which is the eigenvalue of the \hat{J}_z operator.

Conservation of magnetization M has a direct consequence on the equilibrium states of the spinor condensate [27]. The general quantum state $\hat{\rho}$ takes the block-diagonal structure [9, 41]

$$\hat{\rho} = \sum_{M=-N}^N w_M \hat{\rho}_M, \quad (2)$$

where $\hat{\rho}_M = \hat{P}_M e^{-\beta \hat{H}} \hat{P}_M / \mathcal{Z}_M$ is a thermal state in the subspace of fixed magnetization M , with projection operator \hat{P}_M , and \mathcal{Z}_M is the partition function ensuring $\text{Tr}\{\hat{\rho}_M\} = 1$. The temperature T is controlled by the parameter $\beta = \tilde{c}/(k_B T)$, where k_B is the Boltzmann constant. The non-thermal weights $w_M = \exp[-(M - \bar{M})^2/2\sigma^2]/Z$, where $Z = \sum_M \exp[-(M - \bar{M})^2/2\sigma^2]$, reflect our control over the magnetization before thermalization. The average value of magnetization is $\bar{M} = \langle \hat{J}_z \rangle$ while fluctuations of magnetization are set by $\sigma \simeq \sqrt{\langle \hat{J}_z^2 \rangle - \langle \hat{J}_z \rangle^2}$.

The three magnetically sensitive Zeeman states can be used to encode information about unknown physical quantities, that can be subsequently extracted using quantum interferometry techniques. In [9] the authors characterized metrological usefulness of quantum states defined in Eq. (2) for generalized three-mode linear interferometry using the quantum Fisher Information (QFI). Whenever magnetization can be well controlled, $\sigma < 1$, both ground states and mixed by the temperature states provide Heisenberg-like scaling of the QFI, irrespective of the magnetization value. However, as noted in [9] fluctuations of magnetization reduce the QFI but the sub-SQL value preserves when $\sigma < \sqrt{N}$. The authors emphasize that the quantum interferometer which provides optimal value of the QFI is relatively simple due to symmetry of the states (2).

The output state of the three-mode interferometer with equal phase difference θ between neighboring paths can be written in general as $\hat{\rho}_{\text{out}} = e^{-i\theta \hat{\Lambda}_n} \hat{\rho} e^{i\theta \hat{\Lambda}_n}$, where $\hat{\rho}$ is the input density matrix and $\hat{\Lambda}_n = \hat{\Lambda} \cdot \mathbf{n}$ is a generator of rotation, with a unit length vector \mathbf{n} and a vector of generators $\hat{\Lambda} = \{\hat{J}_x, \hat{Q}_{zx}, \hat{J}_y, \hat{Q}_{yz}, \hat{D}_{xy}, \hat{Q}_{xy}, \hat{Y}, \hat{J}_z\}$,

¹ The system considered consists of a few thousand atoms in which creation of spin domains are energetically costly (spin healing length is much larger than the linear system size). Therefore, in the low temperature limit all atoms share the same spatial wave function and the spatial and spin degrees of freedom can be decoupled.

² The magnetization $M = \langle \hat{J}_z \rangle$ longitudinal with respect to magnetic field is approximately conserved in the system and acts as an independent external parameter. The conservation law of magnetization comes from the spin rotational symmetry of contact interactions when dipole-dipole interactions are neglected. Therefore, the linear Zeeman energy is irrelevant as it is proportional to the conserved magnetization, while essential becomes the quadratic Zeeman energy which is given by $-q\hat{N}_0$, where

$q = Q/\tilde{c}$ and $Q = (\mu_B \mathcal{B})^2 / (4E_{\text{hf}})$ depends on the magnetic field strength \mathcal{B} , the Bohr magneton μ_B and the hyperfine energy splitting E_{hf} which can be both positive and negative [39, 40].

spanning the bosonic SU(3) Lie algebra:

$$\hat{J}_x = \frac{1}{\sqrt{2}} (\hat{a}_{-1}^\dagger \hat{a}_0 + \hat{a}_0^\dagger \hat{a}_{-1} + \hat{a}_0^\dagger \hat{a}_1 + \hat{a}_1^\dagger \hat{a}_0), \quad (3)$$

$$\hat{Q}_{zx} = \frac{1}{\sqrt{2}} (-\hat{a}_{-1}^\dagger \hat{a}_0 - \hat{a}_0^\dagger \hat{a}_{-1} + \hat{a}_0^\dagger \hat{a}_1 + \hat{a}_1^\dagger \hat{a}_0), \quad (4)$$

$$\hat{J}_y = \frac{i}{\sqrt{2}} (\hat{a}_{-1}^\dagger \hat{a}_0 - \hat{a}_0^\dagger \hat{a}_{-1} + \hat{a}_0^\dagger \hat{a}_1 - \hat{a}_1^\dagger \hat{a}_0), \quad (5)$$

$$\hat{Q}_{yz} = \frac{i}{\sqrt{2}} (-\hat{a}_{-1}^\dagger \hat{a}_0 + \hat{a}_0^\dagger \hat{a}_{-1} + \hat{a}_0^\dagger \hat{a}_1 - \hat{a}_1^\dagger \hat{a}_0), \quad (6)$$

$$\hat{D}_{xy} = \hat{a}_{-1}^\dagger \hat{a}_1 + \hat{a}_1^\dagger \hat{a}_{-1}, \quad (7)$$

$$\hat{Q}_{xy} = i (\hat{a}_{-1}^\dagger \hat{a}_1 - \hat{a}_1^\dagger \hat{a}_{-1}), \quad (8)$$

$$\hat{Y} = \frac{1}{\sqrt{3}} (\hat{a}_{-1}^\dagger \hat{a}_{-1} - 2\hat{a}_0^\dagger \hat{a}_0 + \hat{a}_1^\dagger \hat{a}_1), \quad (9)$$

$$\hat{J}_z = \hat{a}_1^\dagger \hat{a}_1 - \hat{a}_{-1}^\dagger \hat{a}_{-1}, \quad (10)$$

where \hat{a}_{m_F} is annihilation operator of particle in the m_F Zeeman component. In the case of three-mode interferometer, the phase θ for example can be proportional to the magnetic field strength owing to the linear Zeeman effect [9].

For macroscopic magnetization, i.e. $M = O(N)$ and $N - M = O(N)$, the optimal QFI was shown [9] to be $F_Q = 4\max(\lambda_A, \lambda_B)$, with

$$\lambda_A = \Gamma_{66}, \quad (11)$$

$$\lambda_B = \left(\Gamma_{33} + \Gamma_{44} + \sqrt{4\Gamma_{34}^2 + (\Gamma_{33} - \Gamma_{44})^2} \right) / 2, \quad (12)$$

where elements of the covariance matrix Γ are defined as follows

$$\begin{aligned} \Gamma_{i,j}[\hat{\rho}] &= \sum_k v_k \left[\frac{1}{2} \langle k | \{ \hat{\Lambda}_i, \hat{\Lambda}_j \} | k \rangle - \langle k | \hat{\Lambda}_i | k \rangle \langle k | \hat{\Lambda}_j | k \rangle \right] \\ &\quad - 4 \sum_{k>l} \frac{v_k v_l}{v_k + v_l} \text{Re} \left[\langle k | \hat{\Lambda}_i | l \rangle \langle k | \hat{\Lambda}_j | l \rangle \right], \end{aligned} \quad (13)$$

with eigenvalues v_k and eigenvectors $|k\rangle$ of the input density matrix operator $\hat{\rho} = \sum v_k |k\rangle \langle k|$. The maximal possible value of the QFI is $F_Q = 4N^2$ and sets the Heisenberg limit for the estimation precision $\Delta\theta$, that can be attained only by the fully particle entangled states. On the other hand, separable states can give at most $F_Q = 4N$. The factor 4 in the scaling of characteristic limits of the QFI is due to the su(3) Lie algebra (the extensions from qubits to qudits for corresponding scaling can be found in [20, 42]). In general, for separable qudit states $F_Q[\hat{\rho}_{sep}] \leq N(h_{\max} - h_{\min})^2$ while for entangled states $F_Q[\hat{\rho}] \leq N^2(h_{\max} - h_{\min})^2$, where h_{\max} and h_{\min} are the maximal and minimal eigenvalues of the single qudit Hamiltonian, respectively. In the case of qutrits (three-mode case) one has $h_{\max} = 1$ and $h_{\min} = -1$ whereas for qubits (two-mode case) $h_{\max} = 1/2$ and $h_{\min} = -1/2$.

Optimal value of the QFI can be attained when particular interferometer, defined by the operator $\hat{\Lambda}_{\mathbf{n}}$, is used. When the QFI is determined by the value of λ_A (or λ_B),

the rotation $e^{-i\theta\hat{\Lambda}_{\mathbf{n}}^{(A)}}$ (or $e^{-i\theta\hat{\Lambda}_{\mathbf{n}}^{(B)}}$) optimizes the QFI, where

$$\hat{\Lambda}_{\mathbf{n}}^{(A)} = \hat{Q}_{xy}, \quad (14)$$

and

$$\begin{aligned} \hat{\Lambda}_{\mathbf{n}}^{(B)} &= \frac{1}{\sqrt{\mathcal{N}}} (\hat{J}_y + \gamma \hat{Q}_{yz}) \\ &= \frac{i(1-\gamma)}{\sqrt{2\mathcal{N}}} (\hat{a}_{-1}^\dagger \hat{a}_0 - \hat{a}_0^\dagger \hat{a}_{-1}) + \frac{i(1+\gamma)}{\sqrt{2\mathcal{N}}} (\hat{a}_0^\dagger \hat{a}_1 - \hat{a}_1^\dagger \hat{a}_0) \end{aligned} \quad (15)$$

with

$$\gamma = (\Gamma_{44} - \Gamma_{33} + \sqrt{4\Gamma_{34}^2 + (\Gamma_{33} - \Gamma_{44})^2}) / (2\Gamma_{34}), \quad (16)$$

and $\mathcal{N} = 1 + \gamma^2$. Although the covariance matrix (13) has a complicated form, in general, the QFI is given by the variance of $\hat{\Lambda}^{(A,B)}$ as long as fluctuations of magnetization are negligible ($\sigma \rightarrow 0$). This property stems from the fact that generators of the rotation change magnetization and thus the second term in Eq. (13) vanishes.

TABLE I. The expressions for the quantum Fisher information F_Q and the optimal generator of interferometer rotation $\hat{\Lambda}_{\mathbf{n}}$ when magnetization is macroscopic, i.e. $M = O(N)$ and $N - M = O(N)$.

	$\beta \rightarrow \infty, q < q_{th}$	$\beta \rightarrow \infty, q > q_{th}$	$\beta \rightarrow 0, \text{ any } q$
F_Q	$4\lambda_A$	$4\lambda_B$	$4\lambda_B$
$F_Q(\sigma \rightarrow 0)$	$4\langle (\hat{\Lambda}_{\mathbf{n}}^{(A)})^2 \rangle$	$4\langle (\hat{\Lambda}_{\mathbf{n}}^{(B)})^2 \rangle$	$4\langle (\hat{\Lambda}_{\mathbf{n}}^{(B)})^2 \rangle$
$\hat{\Lambda}_{\mathbf{n}}$	$\hat{\Lambda}_{\mathbf{n}}^{(A)}$	$\hat{\Lambda}_{\mathbf{n}}^{(B)}$	$\hat{\Lambda}_{\mathbf{n}}^{(B)}$

The diagram of the optimal QFI as a function of q and β , for a fixed M , is very regular. It consists of three regions where the optimal interferometer is either $\hat{\Lambda}^{(A)}$ or $\hat{\Lambda}^{(B)}$ as summarized in Table I. In the zero temperature limit ($\beta \rightarrow \infty$), the optimal interferometer is $\hat{\Lambda}_{\mathbf{n}}^{(A)}$ for $q < q_{th}$ and changes into $\hat{\Lambda}_{\mathbf{n}}^{(B)}$ in the opposite case. The threshold value q_{th} defines a degenerate point where both operators give the same value of the QFI. The zero-temperature behavior of the QFI extends deep into non-zero temperature regime. When the thermal energy dominates the QFI saturates at a finite value and does not depend on q , giving rise to a third region with optimal interferometer $\hat{\Lambda}_{\mathbf{n}}^{(B)}$. The optimal interferometer involves two modes $m_F = \pm 1$ only in the region A, what is not the case for B in general. However, when $|\gamma| = 1$ the optimal interferometer in the region B is two-mode as well, e.g. $m_F = 0, 1$ for positive average magnetizations. Therefore, we distinguish between three-mode interferometer $\hat{\Lambda}_{\mathbf{n}}^{(B)}$, with proper value of γ and the two-mode interferometer $\hat{K}_y = i(\hat{a}_0^\dagger \hat{a}_{+1} - \hat{a}_{-1}^\dagger \hat{a}_0)$, with $\gamma = 1$ in the definition n Eq. (15) (as we concentrate on positive average magnetizations $\langle \hat{J}_z \rangle > 0$).

III. ATOMIC MAGNETOMETRY

Magnetometers based on alkali atoms rely on the detection of Larmor precession. For a weak magnetic field oriented along the z-axis, the collective quantum state $\hat{\rho}_r$ acquires a phase $\theta = \mathcal{S}Bt_{\text{hold}}$, during a hold time t_{hold} . The sensitivity \mathcal{S} relates Larmor frequency $\omega = \mathcal{S}B$ to the magnetic field strength B [43]. During the Larmor precession cycle, the state $\hat{\rho}_r$ is rotated around operator \hat{J}_z according to the equation

$$\hat{\rho}_r(\theta) = e^{i\theta\hat{J}_z}\hat{\rho}_r e^{i\theta\hat{J}_z}. \quad (17)$$

The states (2) of spin-1 Bose-Einstein condensates are optimally employed if the interferometer is either $\hat{\Lambda}_{\mathbf{n}}^{(A)}$ or $\hat{\Lambda}_{\mathbf{n}}^{(B)}$. This can be done using current technology in a three stage interferometer with phase imprinting process defined in Eq. (17). During a preparation procedure the input quantum state $\hat{\rho}$ is rotated using unitary operator \hat{R} , resulting in $\hat{\rho}_r = \hat{R}\hat{\rho}\hat{R}^\dagger$. Subsequently, the state $\hat{\rho}_r$ is subject to a phase imprinting process (17). Finally, the state $\hat{\rho}_r(\theta)$ is dis-entangled using conjugate rotation \hat{R}^\dagger giving $\hat{\rho}_\theta = \hat{R}^\dagger\hat{\rho}_r(\theta)\hat{R}$. In order to implement a general rotation $\exp(-i\theta\hat{\Lambda}_{\mathbf{n}})$ we need to find a unitary transformation \hat{R} such that

$$\hat{R}^\dagger e^{-i\theta\hat{J}_z} \hat{R} = e^{-i\theta\hat{\Lambda}_{\mathbf{n}}}. \quad (18)$$

It is a straightforward procedure for $\hat{\Lambda}_{\mathbf{n}} = \hat{\Lambda}_{\mathbf{n}}^{(A)} = \hat{Q}_{xy}$, because operators $\{\hat{D}_{xy}, \hat{Q}_{xy}, \hat{J}_z\}$ span the SU(2) Lie algebra, thus $\hat{R} = \exp(-i\pi\hat{D}_{xy}/4)$. In the second case, with $\hat{\Lambda}_{\mathbf{n}} = \hat{\Lambda}_{\mathbf{n}}^{(B)} = (\hat{J}_y + \gamma\hat{Q}_{yz})/\sqrt{1+\gamma^2}$, we need two rotations $\hat{R} = \exp(-i\pi\hat{J}_x/2)\exp(i\alpha\hat{Q}_{xy})$, where $\cos\alpha = (1+\gamma^2)^{-1/2}$. Both rotations can be realized experimentally, since they either involve two extremal modes $m_F = \pm 1$ or spin operators [3, 44].

IV. THE FISHER INFORMATION

A large value of the QFI implies that the quantum state $\hat{\rho}$ may be useful for sub-SQL interferometry as long as a proper quantum measurement and an estimator are chosen. Finding the optimal measurement, which at the same time is experimentally implementable, is not a straightforward task. A collection of measurement operators $\hat{\Pi}_x$, satisfying $\sum_x \hat{\Pi}_x \hat{\Pi}_x = \mathbb{1}$, defines a conditional probabilities $p(x|\theta) = \text{Tr}\{\hat{\Pi}_x \hat{\rho}_{\text{out}}\}$ of measuring the outcome x given the θ . The knowledge of $p(x|\theta)$ is used to construct an estimator for the phase θ , and according to the Cramér-Rao inequality, the precision $\Delta\theta$ in the θ estimation is bounded from below by the Fisher information $\mathcal{I}(\theta)$ defined as [24, 45]

$$\mathcal{I}(\theta) = \sum_x \frac{1}{p(x|\theta)} \left(\frac{\partial p(x|\theta)}{\partial \theta} \right)^2. \quad (19)$$

An equivalent formulas for the FI can be found in Appendix A. The FI is always smaller than the QFI, i.e. $\mathcal{I}(\theta) \leq F_Q$, because the QFI is already optimized over all possible quantum measurements [25]. Suggesting a measurement $\hat{\Pi}_x$ that would saturate this inequality is a relevant theoretical task for practical implementation. As noted [46, 47], there always exists a projective measurement strategy in the eigenbasis of the symmetric logarithmic derivative [25, 45] that is optimal, but it is θ -dependent and typically not straightforward.

Our choice is the experimentally relevant measurement of populations of Zeeman components and purpose of our calculations is to verify if and when this measurement is optimal, i.e. maximize the FI up to its quantum value. We define the operator of measurement as $\hat{\Pi}_{\{M,k\}} = |M,k\rangle\langle M,k|$, with the Fock state $|M,k\rangle \equiv |N_{+1}, N_0, N_{-1}\rangle$, with constraint imposed on the total particle number $\sum_{m_F} N_{m_F} = N$, the magnetization $N_{+1} - N_{-1} = M$ and the occupation of the $m_F = +1$ component $k = N_{+1}$. The occupation of the $m_F = +1$ Zeeman component depends on the magnetization $k = k_{\min}, \dots, k_{\max}$, where $k_{\min} = \max(0, M)$ and $k_{\max} = \lfloor (N+M)/2 \rfloor$. The probability distribution $p(\{M,k\}|\theta)$ is then

$$p(\{M,k\}|\theta) = \langle M,k | e^{-i\theta\hat{\Lambda}_{\mathbf{n}}} \hat{\rho} e^{i\theta\hat{\Lambda}_{\mathbf{n}}} | M,k \rangle. \quad (20)$$

In the parametrization we introduced, the general quantum states (2) can be written as

$$\hat{\rho} = \sum_{M'} w_{M'} \sum_{k_1, k_2} \rho_{k_1, k_2}^{M'} |M', k_1\rangle\langle M', k_2| \quad (21)$$

and the probability distribution (20) is equal to

$$p(\{M,k\}|\theta) = \sum_{M'} w_{M'} \sum_{k_1, k_2} \rho_{k_1, k_2}^{M'} \left[\mathcal{D}_{k_1, k}^{M', M}(\hat{\Lambda}_{\mathbf{n}}, \theta) \right]^* \mathcal{D}_{k_2, k}^{M', M}(\hat{\Lambda}_{\mathbf{n}}, \theta), \quad (22)$$

where $\mathcal{D}_{k', k}^{M', M}(\hat{\Lambda}_{\mathbf{n}}, \theta) = \langle M', k' | e^{i\theta\hat{\Lambda}_{\mathbf{n}}} | M, k \rangle$.

A. Ground states and fixed magnetization

We start our analysis with the simplest case of the pure state $|\Psi_{\bar{M}}\rangle$ in the block of fixed magnetization \bar{M} . It means that the distribution of magnetization is just $w_M = \delta_{\bar{M}, M}$. We denote the rotated pure state by $|\Psi_{\bar{M}}\rangle_\theta \equiv e^{-i\theta\hat{\Lambda}_{\mathbf{n}}} |\Psi_{\bar{M}}\rangle$ which expanded over the Fock state basis is $|\Psi_{\bar{M}}\rangle_\theta = \sum_{M,k} C_{M,k}(\theta) |M,k\rangle$. Expansion coefficients $C_{M,k}(\theta)$ are all real, because both the state $|\Psi_{\bar{M}}\rangle$ and the rotation with $\hat{\Lambda}_{\mathbf{n}}^{(A,B)}$ are real. Conditional probability is equal to $p(\{M,k\}|\theta) = C_{M,k}^2(\theta)$. Since, probability is determined by a single real number one can show that the FI equals to [48]

$$\mathcal{I}(\theta) = 4\langle \Psi_{\bar{M}} | \hat{\Lambda}_{\mathbf{n}}^2 | \Psi_{\bar{M}} \rangle. \quad (23)$$

The FI (23) has the same form as the QFI [9]. Moreover, the measurement of populations of Zeeman components is optimal for any value of θ . It holds for both the three- and -two mode interferometers. We mentioned that operators $\hat{\Lambda}_n^{(A,B)}$ give optimal value of the QFI for macroscopic magnetization, but in fact they are also good in the case $M = 0$. The slight difference is, that for $c_2 < 0$ the optimal operator can be \hat{J}_y ($\gamma = 0$ in $\hat{\Lambda}_n^{(B)}$) for some values of magnetic field, see Section V.

We verified our finding by numerical calculations within exact diagonalization method, see Appendix B for explanation. An example of numerical results is shown in Fig.1 demonstrating validity of the analytical analysis.

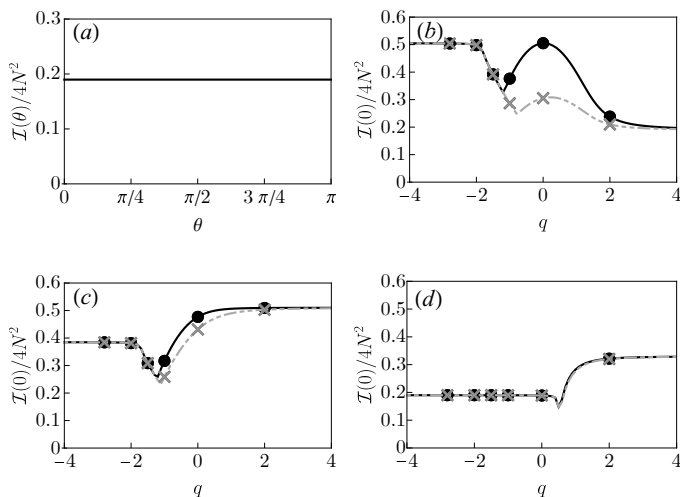


FIG. 1. An example of the FI from (19) divided by $4N^2$ versus θ from exact numerical calculations for $M = 0.8N$, $q = 0$ and $c_2 > 0$ is shown in (a). The FI at $\theta = 0$ versus q for the three-mode (black circles) and two-mode (gray crosses) interferometry compared to the QFI for the three-mode (black solid lines) and two-mode (gray dashed lines) interferometry in the ground state of the system for fixed magnetization $M = 0.1N$ and $c_2 < 0$ in (b), $M = 0.5N$ and $c_2 < 0$ in (c), and $M = 0.8N$ and $c_2 > 0$ in (d). The total atom number is $N = 10^2$.

B. Thermal states and fixed magnetization

When the temperature is non-zero, but the state still has a well defined magnetization ($\sigma \rightarrow 0$), the general quantum state (2) can be written down in the Fock state basis as follows

$$\hat{\rho} = \sum_{k_1, k_2} \rho_{k_1, k_2}^{\bar{M}} |\bar{M}, k_1\rangle \langle \bar{M}, k_2|. \quad (24)$$

In general, when the information about θ is encoded on three modes, e.g. by rotation around $\hat{\Lambda}_n^{(B)}$, analytical expressions for the FI can be derived only at $\theta = 0$.

The probability $p(\{M, k\}|0) = \rho_{k_1, k_1}^{\bar{M}} \delta_{\bar{M}, M} \delta_{k_1, k}$ is non-zero only for limited values of $\{M, k\}$. On the other hand, the first derivative

$$\left. \frac{\partial p(\{M, k\}|\theta)}{\partial \theta} \right|_{\theta=0} = \sum_{k_1, k_2} \rho_{k_1, k_2}^{\bar{M}} \delta_{\bar{M}, M} \cdot \left\{ \langle \bar{M}, k_1 | (i\hat{\Lambda}_n) | M, k \rangle^* \delta_{k_2, k} + \langle M, k_2 | (i\hat{\Lambda}_n) | \bar{M}, k \rangle \delta_{k_1, k} \right\} \quad (25)$$

is always zero for operators $\hat{\Lambda}_n^{(A,B)}$, because they do change magnetization. Whenever $p(\{M, k\}|0) \rightarrow 0$ one has to analyze the $0/0$ expression, e.g. using l'Hospital's rule. In that case, the FI is determined by the second derivative of the probability $p(\{M, k\}|\theta)$ taken at $\theta \rightarrow 0$, what gives

$$\begin{aligned} \mathcal{I}(0) = & 4 \sum_{k_1, k_2} \rho_{k_1, k_2}^{\bar{M}} \langle \bar{M}, k_2 | \hat{\Lambda}_n^2 | \bar{M}, k_1 \rangle \\ & - 4 \sum_k \sum_{k_1, k_2} \rho_{k_1, k_2}^{\bar{M}} \langle \bar{M}, k | \hat{\Lambda}_n | \bar{M}, k_1 \rangle \langle \bar{M}, k_2 | \hat{\Lambda}_n | \bar{M}, k \rangle, \end{aligned} \quad (26)$$

where the summation runs over all indexes for which $\rho_{k, k}^{\bar{M}} \neq 0$. The operators $\hat{\Lambda}_n$ that do not change magnetization, e.g. $\hat{\Lambda}_n = \hat{J}_z$ or \hat{Y} , give $\mathcal{I}(0) = 0$ due to compensation of both terms in Eq. (26). Luckily, for operators $\hat{\Lambda}_n^{(A,B)}$ the second term in (26) vanishes and the FI equals the QFI, see Table I. However, the θ dependence of the FI is in general unknown and, therefore, numerical calculations are needed.

By performing and analyzing exact numerical results we made the following observations. In general, the FI for the three-mode interferometer do depend on the phase θ taking maximal value for $\theta = 0, \pm\pi, \dots$ (see example in Fig. 2(a)). We noticed that a variation of $\mathcal{I}(\theta)$ versus θ strongly depends on the value of q . In the vicinity of the threshold point q_{th} the FI strongly depends on θ (as demonstrated in Fig. 2(a)). The farther away from the q_{th} , the smaller the changes, which eventually give $\mathcal{I}(\theta) \rightarrow \mathcal{I}(0)$ when $|q| \gg q_{th}$. In the high magnetic field limit, $q \rightarrow \infty$, the FI for the two-mode transformations are equal to the FI for the three-mode interferometers, and they are θ independent. This observation suggests that the two-mode interferometers may in general give the FI independent of θ . Indeed, we confirmed both numerically (see Fig. 2) and analytically (see Section IV B 1) that the FI and the QFI have the same value for the two-mode interferometers and they are independent of θ . We explain that surprising at the first look result for our system in Section IV B 1 and generalize to the systems composed of atoms with higher spin in Section IV B 2. In Fig. 2 we gathered exact numerical results for a broad range of parameters. An exemplary variation of $\mathcal{I}(\theta)$ with θ is shown in (a) for q close to the threshold value q_{th} for the ferromagnetic case $c_2 < 0$. A comparison of the QFI value to the maximal value of FI is shown in (b)-(d), also

demonstrating that the two-mode interferometer transformation is competitive with the three-mode one and gives the HL of the FI in a broad range of parameters.

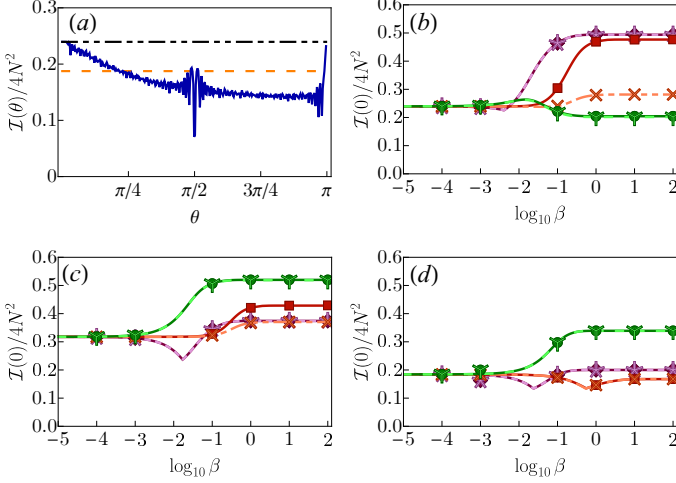


FIG. 2. (a) An example of θ dependence of the FI from (19) divided by $4N^2$ for $\hat{\Lambda}_{\mathbf{n}} = \hat{\Lambda}_{\mathbf{n}}^{(A)}$ (orange dashed line), the two-mode $\hat{\Lambda}_{\mathbf{n}} = \hat{K}_y$ (black dash-dotted line) and the three-mode $\hat{\Lambda}_{\mathbf{n}} = \hat{\Lambda}_{\mathbf{n}}^{(B)}$ (blue solid line) interferometric transformations with $M = 0.1N$, $\beta = 10^{-3}$, $q = -0.5$, $c_2 < 0$. In (b)-(d) the two-mode (crossed points) and the three-mode (filled points) versions of the FI divided by $4N^2$ versus $\log_{10}\beta$ are shown and compared to the two-mode (dashed lines) and three-mode (solid lines) versions of the QFI divided by $4N^2$ for different values of q as indicated by colors: $q = -5$ (marked by purple), $q = -0.5$ if $c_2 < 0$ or $q = 0.5$ if $c_2 > 0$ (marked by red) and $q = 5$ (marked by green). The parameters are $M = 0.1N$, $c_2 < 0$ in (b), $M = 0.5N$, $c_2 < 0$ in (c), $M = 0.8N$, $c_2 > 0$ in (d) with $N = 50$.

1. Mapping to the $SU(2)$

When the unknown value of θ is encoded only in two modes, the third mode carries no information about θ and any measurement involving that mode does not increase the FI value. The interferometric precision is the same as for the initial quantum state $\hat{\rho}$ traced out over the unused mode $\hat{\rho}_2 = \text{Tr}_3\{\hat{\rho}\}$. This is a general statement and is not limited to the three-mode case. Any n_{arb} -mode state $\hat{\rho}_{n_{\text{arb}}}$ gives the same statistics, in a two-mode interferometry, as the two-mode state $\hat{\rho}_2 = \text{Tr}_{n_{\text{arb}}-2}\{\hat{\rho}_{n_{\text{arb}}}\}$, where the trace is taken over $n_{\text{arb}} - 2$ unused modes.

In order to demonstrate that the measurement of populations of Zeeman components is optimal for a two-mode interferometric transformation we focus on the two $m_F = \pm 1$ states (similar calculations can be done for other combinations). The triple operators $\hat{A}_x = \hat{D}_{xy}$, $\hat{A}_y = \hat{Q}_{xy}$ and $\hat{A}_z = \hat{J}_z$ span the $SU(2)$ Lie algebra with cyclic commutation relations $[\hat{A}_n, \hat{A}_k] = 2i\epsilon_{nkl}\hat{A}_l$. The Fock state $|N_{+1}, N_0, N_{-1}\rangle$ is a simultaneous eigenstate of $\hat{A}^2 = \sum_i \hat{A}_i^2$, with eigenvalue $4j(j+1)$ where

$2j = N_{+1} + N_{-1}$ and \hat{A}_z , with eigenvalue $2m$ where $2m = N_{+1} - N_{-1}$. In the two-mode spirit, one can parametrize the Fock state as $|j+m, N-2j, j-m\rangle$. The quantum state limited to the fixed magnetization subspace can be then written in the following form

$$\hat{\rho} = \sum_{j_1, j_2} C_{j_1, j_2} |j_1 + \bar{m}, N - 2j_1, j_1 - \bar{m}\rangle \times \langle j_2 + \bar{m}, N - 2j_2, j_2 - \bar{m}|. \quad (27)$$

In the two-mode interferometric transformation $\exp(-i\theta\hat{A}_y)$ the third mode $m_F = 0$ carries no information about θ , thus we can work with reduced quantum state

$$\hat{\rho}_2 = \text{Tr}_0\{\hat{\rho}\} = \sum_j C_{j, j} |j, \bar{m}\rangle \langle j, \bar{m}|, \quad (28)$$

where shorthand notation $|j, \bar{m}\rangle \equiv |j + \bar{m}, j - \bar{m}\rangle$ was used. Probability of measuring N_{+1} atoms in the $m_F = 1$ component and N_{-1} atoms in the $m_F = -1$ component is equivalent to calculating $p(\{j, m\}|\theta) = \langle j, m|\hat{\rho}_2(\theta)|j, m\rangle$, where $\hat{\rho}_2(\theta) = \exp(-i\theta\hat{A}_y)\hat{\rho}_2\exp(i\theta\hat{A}_y)$. This is a typical Mach-Zehnder interferometer and straightforward calculation gives

$$p(\{j, m\}|\theta) = C_{j, j} [d_{m, \bar{m}}^{(j)}(2\theta)]^2, \quad (29)$$

where $d_{m, \bar{m}}^{(j)}(2\theta) = \langle j, m|e^{-i\theta\hat{A}_y}|j, \bar{m}\rangle$ is the Wigner rotation matrix. The FI is [48]

$$\begin{aligned} \mathcal{I}(\theta) &= 4 \sum_{j, m} C_{j, j} \left[\frac{d}{d\theta} d_{m, \bar{m}}^{(j)}(2\theta) \right]^2 \\ &= 4 \sum_j C_{j, j} \langle j, m|\hat{A}_y^2|j, m\rangle, \end{aligned} \quad (30)$$

and equals the two-mode QFI with $F_Q = 4(\hat{A}_y^2)$ for any value of the phase θ . The conclusion remains unchanged for other triple operators which involve the $m_F = 0, 1$ or $m_F = 0, -1$ Zeeman components. When the interferometer involves the $m_F = 0, +1$ Zeeman components then the triple operators are $\hat{A}_x = (\hat{J}_x + \hat{Q}_{zx})/\sqrt{2}$, $\hat{A}_y = (\hat{J}_y + \hat{Q}_{yx})/\sqrt{2}$, $\hat{A}_z = (\hat{J}_z + \sqrt{3}\hat{Y})/2$. The corresponding Fock state can be re-expressed as $|j+m, j-m, N-2j\rangle$ and $m = M + N - 3j$. When the interferometer involves the $m_F = 0, -1$ Zeeman modes then $\hat{A}_x = (\hat{J}_x - \hat{Q}_{zx})/\sqrt{2}$, $\hat{A}_y = (\hat{J}_y - \hat{Q}_{yx})/\sqrt{2}$, $\hat{A}_z = (\hat{J}_z - \sqrt{3}\hat{Y})/2$ and the corresponding Fock state can be re-expressed as $|N-2j, j+m, j-m\rangle$ with $m = M + N + 3j$.

2. Efficiency of the two-mode interferometer for an arbitrary number of input modes

In the case of n_{arb} number of input modes, the general mixed quantum state can be written as

$$\hat{\rho} = \sum_{j, j'} \sum_{m, m'} \sum_{\mathbf{l}, \mathbf{l}'} C_{j, m, \mathbf{l}}^{j', m', \mathbf{l}'} |j+m, j-m, \mathbf{l}\rangle \langle j'+m', j'-m', \mathbf{l}'|, \quad (31)$$

where $j \in \{0, 1/2, \dots, N/2\}$, $m \in \{-j, -j+1, \dots, j\}$ and $\mathbf{l} = (l_1, \dots, l_{n_{\text{arb}}-2})$ with $\sum_{i=1}^{n_{\text{arb}}-2} l_i = n_{\text{arb}} - 2j$. Since $n_{\text{arb}} - 2$ modes do not take part in the interferometry operation we can trace them out and effectively work with

$$\hat{\rho}_2 = \text{Tr}_1[\hat{\rho}] = \sum_j \sum_{m, m'} \rho_{m, m'}^j |j+m, j-m\rangle \langle j+m', j-m'|, \quad (32)$$

where $\rho_{m, m'}^j = \sum_{\mathbf{l}} C_{j, m, \mathbf{l}}^{j, m', \mathbf{l}}$. If it happens that $\hat{\rho}$ encloses itself entirely in a subspace with fixed $m = \bar{m}$, or at least m can be written as a function of j , i.e. $m = m(j)$, then

$$\hat{\rho}_2 = \sum_j \rho_{m(j), m(j)}^j |j+m(j), j-m(j)\rangle \langle j+m(j), j-m(j)|, \quad (33)$$

and it is an incoherent mixture of pure states belonging to different subspaces of j . Because the two-mode interferometer \hat{A}_y does not connect states with different quantum number j , then the reduced two-mode quantum Fisher information is

$$F_Q[\hat{\rho}_2] = 8 \sum_j \rho_{m(j), m(j)}^j [j(j+1) - m(j)^2], \quad (34)$$

and based on the results from the previous Section IV B 1, one can also show that the corresponding FI is independent of the phase θ and

$$\mathcal{I}(\theta; \hat{\rho}_2) = F_Q[\hat{\rho}_2]. \quad (35)$$

In general one can map an arbitrary number mode state into the two-mode interferometry by tracing out unused modes, because they do not add any information about the sensitivity of a quantum state to unitary rotations that define the two-mode interferometer.

C. When magnetization fluctuates

Lets us consider the most general states for macroscopic magnetizations with nonzero fluctuations of magnetization $\Delta M = \sigma \neq 0$. The FI can be analyzed analytically for zero temperature only when the ground state in the subspace of fixed magnetization is the Fock state $|M, k_{\text{max}}\rangle$ [9] for $q < 0$. In this case the state (2) is of the form

$$\hat{\rho} = \sum_M w_M |M, k_{\text{max}}\rangle \langle M, k_{\text{max}}|, \quad (36)$$

A tedious calculation of the FI at $\theta \rightarrow 0$ leads to

$$F(0) = 4 \sum_M w_M \langle M, k_{\text{max}} | \hat{\Lambda}_{\mathbf{n}}^2 | M, k_{\text{max}} \rangle - 4 \sum_{M', M} w_{M'} |\langle M', k_{\text{max}} | \hat{\Lambda}_{\mathbf{n}} | M, k_{\text{max}} \rangle|^2. \quad (37)$$

Direct calculations show that $\mathcal{I}(0) = 0$ for the optimal operator $\hat{\Lambda}_{\mathbf{n}} = \hat{D}_{xy}$. However, in general the variation of

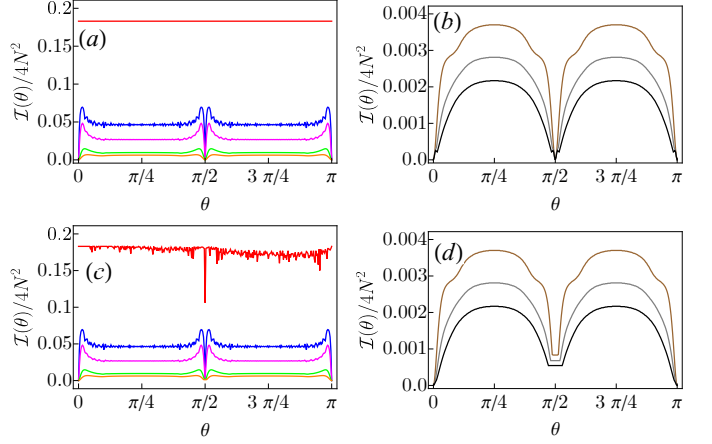


FIG. 3. The FI divided by $4N^2$ from (19) versus θ for the two-mode with $\hat{\Lambda}_{\mathbf{n}} = \hat{K}_y$ in (a)-(b) and three-mode with $\hat{\Lambda}_{\mathbf{n}} = \hat{\Lambda}_{\mathbf{n}}^{(B)}$ in (c)-(d) interferometric transformations including fluctuations of magnetization of amount: $\sigma/\sqrt{N} = 0, \sqrt{2}/20, \sqrt{2}/10, \sqrt{2}/5, 3\sqrt{2}/10$ marked by colored solid lines from top to bottom in (a) and (c), and for $\sigma/\sqrt{N} = \sqrt{2}/2, 7\sqrt{2}/10, \sqrt{2}$ marked by colored solid lines from top to bottom in (b) and (d), with $N = 50, m = 0.1, c_2 > 0, \beta = 10^{-2}$ and $q = 0.5$.

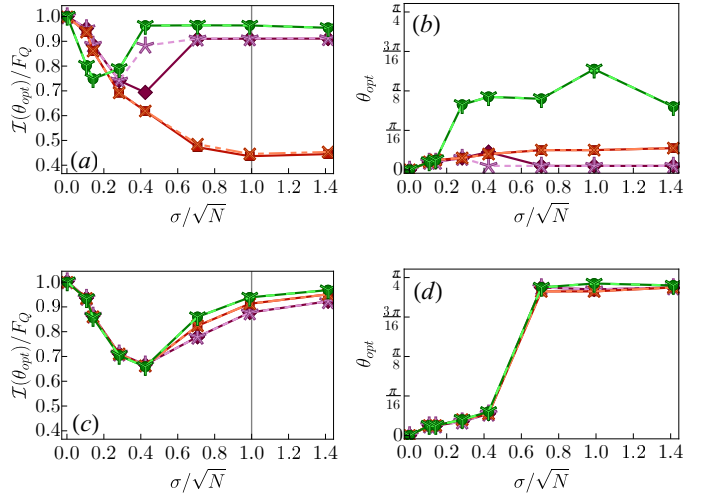


FIG. 4. (a) The maximal value of the relative Fisher information $\mathcal{I}(\theta_{\text{opt}})/F_Q$ versus relative fluctuations of magnetization σ/\sqrt{N} for the two-mode with $\hat{\Lambda}_{\mathbf{n}} = \hat{K}_y$ (crossed points) and the three-mode with $\hat{\Lambda}_{\mathbf{n}} = \hat{\Lambda}_{\mathbf{n}}^{(B)}$ (filled points) interferometry with $q = -5$ (marked by purple stars for the two-mode and by diamonds for the three-mode cases), $q = 0.5$ (marked by red crosses for the two-mode and by squares for the three-mode cases) and $q = 5$ (marked by green "Y" for the two-mode and by circles for the three-mode cases), and for $\beta = 10, N = 50, m = 0.8, c_2 > 0$. (b) θ_{opt} versus σ/\sqrt{N} for the same parameters as in (a). In (c) and (d) the same quantities are plotted as in (a) and (b), respectively, but for $\beta = 10^{-2}$. Vertical lines in (a) and (c) mark SQL. Colored lines linking the points are added to guide the eye.

the FI with θ and its maximal value are unknown. As the above example indicate the optimal value of the FI may not be at $\theta = 0$ anymore. We use numerical calculations to understand the effect of magnetization fluctuations.

An example of our exact numerical results are shown in Fig. 3. Indeed, the resulting FI is equal to 0 when $\theta \rightarrow 0$ but then it increases rapidly with θ , see Fig. 3(a)-(b) for the two-mode and Fig. 3(c)-(d) for the three-mode interferometers. In general, the FI does depend on the phase θ and there is an optimal value of the phase, namely θ_{opt} , for which the FI value is the largest. Thus, fluctuations of magnetization result in a shift of the optimal phase. The similar effect was also observed in the case of detection noise as reported in [49].

In Fig. 4 we gather the maximal values of the $\mathcal{I}(\theta_{\text{opt}})$ in (a) and (c), and corresponding values of θ_{opt} in (b) and (d). Unfortunately, the maximal value of the FI is not exactly equal to the QFI in some cases. It means, that the measurement of populations of Zeeman components is not the most optimal one when fluctuations of magnetization start to play an important role. However, it is not the worst choice because $\mathcal{I}(\theta_{\text{opt}})$ still overcome the standard quantum limit as long as $\sigma < \sqrt{N}$.

V. THE SPECIAL CASE OF ZERO MAGNETIZATION

The authors mentioned in [9] that the optimal value of the QFI is determined by the maximum among the three values: λ_A , λ_B and also $\lambda_C = \Gamma_{77}$ in general. The eigenvalue λ_C corresponds to the optimal interferometric transformation $\hat{\Lambda}_{\mathbf{n}}^{(C)} = \hat{Y}$. In the case of macroscopic magnetization the operators $\hat{\Lambda}_{\mathbf{n}}^{(A,B)}$ were sufficient to determine optimal value of the QFI for all ranges of temperature and magnetic field strength. This is no longer true when M is close to zero in the high temperature limit, where fluctuations of $\hat{\Lambda}_{\mathbf{n}}^{(C)}$ become dominant. In this special case, the QFI of the ground state ($\beta \rightarrow \infty$) is determined by λ_A in the antiferromagnetic phase for $q < q_c$, λ_B in the polar phase for $q > |q_c|$ and by λ_C in the broken axisymmetry phase for $q \in (q_c, |q_c|)$, where q_c is the critical point which at $M = 0$ is $q_c = 0$ for $c_2 > 0$, and $q_c = -2$ for $c_2 < 0$. The situation changes in the high temperature limit ($\beta \rightarrow 0$) when the QFI is determined by the value of λ_C only.

In Fig. 5 we show example of exact numerical results for the FI (points) based on the measurement of populations of Zeeman components compared to the QFI (black solid lines) in the case of zero fluctuations of magnetization ($\sigma \rightarrow 0$). As long as the temperature is low ($\beta \rightarrow \infty$), the measurement of Zeeman components populations is optimal, i.e. maximize the FI. In the high temperature limit ($\beta \rightarrow 0$) the value of λ_C is the highest and determines the value of the QFI. Unfortunately, operator \hat{Y} is diagonal in the Fock state basis and particle number measurement carries no information about θ in

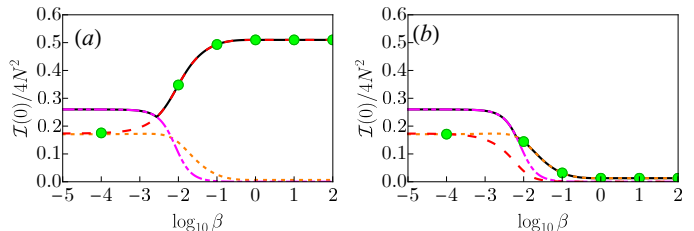


FIG. 5. The FI at $\theta = 0$ (green points) versus $\log_{10} \beta$ for $q = -5$ in (a) and for $q = 5$ in (b) compared to the QFI (black solid line), with $N = 100$, $c_2 < 0$, $\sigma = 0$, $M = 0$. The variances of \hat{D}_{xy} (red dashed line), \hat{J}_x (orange dotted line) and \hat{Y} (purple dot-dashed line) are also shown. All quantities are divided by $4N^2$.

the case of interferometer $\hat{\Lambda}_{\mathbf{n}}^{(C)}$ yielding $\mathcal{I}(\theta) = 0$. Hence, other rotations with ($\hat{\Lambda}_{\mathbf{n}}^{(A)}$ or $\hat{\Lambda}_{\mathbf{n}}^{(B)}$) are a better choice because their variance scales as N^2 .

Interesting situation takes place in the polar phase for $q > 2$. In the ground state all atoms occupy the $m_F = 0$ Zeeman state, forming a coherent state $|0, N, 0\rangle$ with the $F_Q = 4N$. When the temperature grows, higher energy entangled states are being populated increasing the QFI value, as illustrated in Fig.5(b). Finally, in the high-temperature limit ($\beta \rightarrow 0$) the QFI gains the Heisenberg scaling. The careful reader can notice the same effect in Fig.2(d) for macroscopic magnetizations, where the temperature slightly increases the value of the QFI.

VI. PRECISION FROM THE MEASUREMENT OF SIGNAL

The method of moments [45, 50, 51] is a simple estimation strategy, which does not require the knowledge of the probability distribution $p(x|\theta)$. An observable $\hat{\mathcal{P}}$ with θ dependent expectation value $\langle \hat{\mathcal{P}} \rangle_\theta$ carries information about unknown value of θ , and thus can be exploited in the estimation procedure. In the limit of large number of measurements $\nu \gg 1$, the estimation precision $\Delta\theta_{\text{mom}}$ is given by the error-propagation formula [45, 50, 51]: $\Delta\theta_{\text{mom}} = (\Delta\hat{\mathcal{P}})_\theta / |\sqrt{\nu} \partial_\theta \langle \hat{\mathcal{P}} \rangle_\theta|$, where $(\Delta\hat{\mathcal{P}})_\theta = \sqrt{\langle \hat{\mathcal{P}}^2 \rangle_\theta - \langle \hat{\mathcal{P}} \rangle_\theta^2}$. The uncertainty of θ is bounded from below by the QFI

$$(\sqrt{\nu} \Delta\theta_{\text{mom}})^{-2} \leq F_Q. \quad (38)$$

In the two-mode interferometry introduced in Section IVB1, the input states are effectively incoherent mixtures of Dicke states i.e. $\hat{\rho} = \sum_j C_{j,j} |j, m\rangle \langle j, m|$, where $|j, m\rangle \equiv |j+m, j-m\rangle$ is a short-hand notation for the two-mode Fock state with $j+m$ atoms in a state a and $j-m$ in a state b . From now on, we drop any reference to specific Zeeman states and work with general

creation operators \hat{a}^\dagger and \hat{b}^\dagger and spin operators

$$\hat{S}_x = \frac{1}{2}(\hat{a}^\dagger \hat{b} + \hat{b}^\dagger \hat{a}), \quad (39a)$$

$$\hat{S}_y = \frac{1}{2i}(\hat{a}^\dagger \hat{b} - \hat{b}^\dagger \hat{a}), \quad (39b)$$

$$\hat{S}_z = \frac{1}{2}(\hat{a}^\dagger \hat{a} - \hat{b}^\dagger \hat{b}), \quad (39c)$$

which satisfy cyclic commutation relations $[\hat{S}_n, \hat{S}_k] = i\epsilon_{nkl}\hat{S}_l$. It was noted [52] that the measurement of \hat{S}_z^2 operator saturates the inequality (38) for specific value of θ . As we will demonstrate, this result holds only for Dicke states with $m = 0$. Otherwise, the precision $\Delta\theta_{\text{mom}}$ diverges rapidly with m from its optimal value given by the square root inverse of the QFI. We also show, that in the general incoherent mixture the measurement of the parity operator $\hat{\Pi}_b$ does not saturate the inequality (38), but becomes optimal in the case if a single (pure) Dicke state.

A. Measurement of \hat{S}_z^2 operator

In the Mach-Zender interferometer information about θ is imprinted on the initial state $\hat{\rho}$ through a unitary transformation $\hat{\rho}_\theta = \hat{U}_\theta \hat{\rho} \hat{U}_\theta^\dagger$, where $\hat{U}_\theta = \exp(-i\theta \hat{S}_y)$. Expectation value of \hat{S}_z^2 equals

$$\begin{aligned} \langle \hat{S}_z^2 \rangle_\theta &= \text{Tr} \left\{ \hat{S}_z^2 e^{-i\theta \hat{S}_y} \hat{\rho} e^{i\theta \hat{S}_y} \right\} \\ &= \cos^2 \theta \langle \hat{S}_z^2 \rangle + \sin^2 \theta \langle \hat{S}_x^2 \rangle - \cos \theta \sin \theta \langle \{ \hat{S}_z, \hat{S}_x \} \rangle, \end{aligned} \quad (40)$$

where we used the formula $\hat{U}_\theta^\dagger \hat{S}_z \hat{U}_\theta = \cos \theta \hat{S}_z - \sin \theta \hat{S}_x$. In the method of moments uncertainty of θ follows from uncertainty of $\langle \hat{S}_z^2 \rangle_\theta$ [50] and takes the form

$$\Delta\theta_{\text{mom}} = \frac{(\Delta \hat{S}_z^2)_\theta}{\sqrt{\nu} \left| \frac{d}{d\theta} \langle \hat{S}_z^2 \rangle_\theta \right|}, \quad \text{for } \nu \gg 1. \quad (41)$$

As explained in [53], and also in Appendix C, the uncertainty $\Delta\theta_{\text{mom}}$ for a special class of quantum states $\hat{\rho}$ becomes

$$\begin{aligned} \nu \Delta\theta_{\text{mom}}^2 &= \\ &= \frac{(\Delta \hat{S}_x^2)^2 f(\theta) + 4 \langle \hat{S}_x^2 \rangle - 3 \langle \hat{S}_y^2 \rangle - 2 \langle \hat{S}_z^2 \rangle (1 + \langle \hat{S}_x^2 \rangle) + 6 \langle \hat{S}_z \hat{S}_x^2 \hat{S}_z \rangle}{4(\langle \hat{S}_x^2 \rangle - \langle \hat{S}_z^2 \rangle)^2}, \end{aligned} \quad (42)$$

where

$$f(\theta) = \left[\frac{(\Delta \hat{S}_z^2)^2}{(\Delta \hat{S}_x^2)^2} \frac{1}{\tan^2 \theta} + \tan^2 \theta \right]. \quad (43)$$

The phase θ_{opt} which minimizes the uncertainty (40) is

$$\tan^2 \theta_{\text{min}} = \frac{\Delta \hat{S}_z^2}{\Delta \hat{S}_x^2}, \quad (44)$$

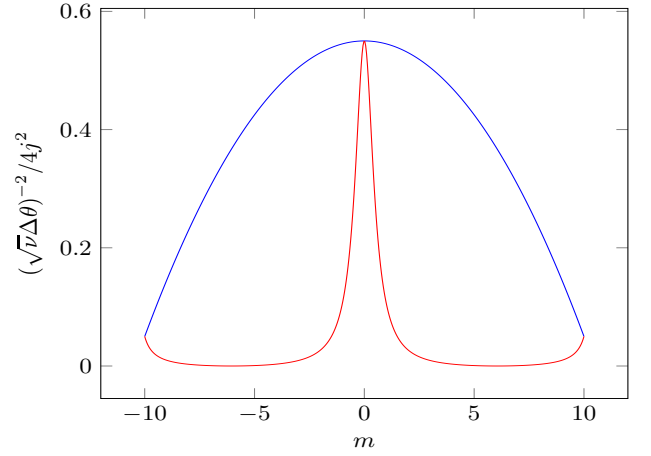


FIG. 6. The precision from the error-propagation formula (50) (red solid) versus the fractional magnetization m compared to the lower bound set by the quantum Fisher information (blue solid).

thus the estimation procedure performed around the value θ_{min} gives the optimal precision $\Delta\theta_{\text{min}}$ with

$$\begin{aligned} \nu \Delta\theta_{\text{min}}^2 &= \\ &= \frac{2\Delta \hat{S}_z^2 \Delta \hat{S}_x^2 + 4 \langle \hat{S}_x^2 \rangle - 3 \langle \hat{S}_y^2 \rangle - 2 \langle \hat{S}_z^2 \rangle (1 + \langle \hat{S}_x^2 \rangle) + 6 \langle \hat{S}_z \hat{S}_x^2 \hat{S}_z \rangle}{4(\langle \hat{S}_x^2 \rangle - \langle \hat{S}_z^2 \rangle)^2}. \end{aligned} \quad (45)$$

For an incoherent mixture of Dicke states $\hat{\rho} = \sum_j C_{j,j} |j, m\rangle \langle j, m|$, introduced in Section IV B 1 we have:

$$\langle \hat{S}_x^2 \rangle = \langle \hat{S}_y^2 \rangle = \frac{1}{2} \sum_j C_{j,j} [j(j+1)] - \frac{1}{2} m^2, \quad (46)$$

$$\langle \hat{S}_z^2 \rangle = m^2, \quad (47)$$

$$\Delta \hat{S}_z^2 = 0, \quad (48)$$

$$\langle \hat{S}_z \hat{S}_x^2 \hat{S}_z \rangle = m^2 \langle \hat{S}_x^2 \rangle, \quad (49)$$

and the inverse of precision squared is equal to

$$(\sqrt{\nu} \Delta\theta_{\text{min}})^{-2} = \frac{2 \left[\sum_j C_{j,j} j(j+1) - 3m^2 \right]^2}{\left[\sum_j C_{j,j} j(j+1) - m^2 \right] (1 + 4m^2) - 4m^2}. \quad (50)$$

The above expression agrees with the QFI value $F_Q[\hat{\rho}] = 2 \sum_j C_{j,j} j(j+1) - 2m^2$ only if m is zero. Otherwise, it diverges rapidly with m as can be seen from the Taylor expansion around small m (see Fig. 6 for special case $\hat{\rho} = |j, m\rangle \langle j, m|$). Therefore, measurement of \hat{S}_z^2 is not the optimal one for the states with macroscopic magnetization which have $m \neq 0$.

B. Mach-Zehnder interferometry with the parity measurement

The parity operator is diagonal in the particle number basis [54]

$$\hat{\Pi} = (-1)^{\hat{N}_b} = \sum_{j,m} (-1)^{j-m} |j, m\rangle \langle j, m|, \quad (51)$$

and has only two eigenvalues ± 1 depending on the particle number parity in the b component. This feature makes it very sensitive to e.q. detection noise [49]. The parity operator can be measured by counting number of particles in one of the components and assigning to this result eigenvalue ± 1 depending on the parity. This requires single particle resolution [55, 56].

Expectation value $\langle \hat{\Pi} \rangle_\theta$ of the parity operator calculated with the initial mixture of Dicke states $\hat{\rho} = \sum_j C_{j,j} |j, m\rangle \langle j, m|$ takes the form

$$\begin{aligned} \langle \hat{\Pi} \rangle_\theta &= \sum_j C_{j,j} \langle j, m | e^{i\theta \hat{S}_y} \cdot \hat{\Pi} \cdot e^{-i\theta \hat{S}_y} |j, m\rangle \\ &= \sum_j C_{j,j} \sum_{m'=-j}^j (-1)^{j-m'} \left| \langle j, m | e^{i\theta \hat{S}_y} |j, m'\rangle \right|^2 \\ &= \sum_j C_{j,j} \sum_{m'=-j}^j (-1)^{j-m'} \left[d_{m,m'}^j(\theta) \right]^2. \end{aligned} \quad (52)$$

Since $\hat{\Pi}^2 = \mathbb{1}$, the error-propagation formula reduces to

$$(\Delta\theta_{\text{mom}} \sqrt{\nu})^{-2} = \frac{\left| \frac{d\langle \hat{\Pi} \rangle_\theta}{d\theta} \right|^2}{1 - \langle \hat{\Pi} \rangle_\theta^2} \leq F_Q[\hat{\rho}] \quad (53)$$

In general, it is not possible to saturate the inequality in Eq. (53) for any coefficients $C_{j,j}$. However, in a special case $\hat{\rho} = |j, m\rangle \langle j, m|$ of a pure Dicke state the 0/0 expression appears in (53) at $\theta = 0$. The Taylor expansion of the expectation value (52) to the 4-th order around small θ gives

$$\langle \hat{\Pi} \rangle_\theta = (-1)^{j-m} \left[1 - \theta^2 \cdot P_2(j, m) + \theta^4 \cdot P_4(j, m) \right], \quad (54)$$

where

$$\begin{aligned} P_2(j, m) &= \langle j, m | \hat{S}_y^2 |j, m\rangle + \sum_{m'} (-1)^{m-m'} \langle j, m | \hat{S}_y |j, m'\rangle^2 \\ &= 2[j(j+1) - m^2] = \frac{F_Q}{2}, \end{aligned} \quad (55)$$

$$\begin{aligned} P_4(j, m) &= \frac{1}{12} \langle j, m | \hat{S}_y^4 |j, m\rangle \\ &+ \frac{1}{3} \sum_{m'} (-1)^{m-m'} \langle j, m | \hat{S}_y |j, m'\rangle \langle j, m | \hat{S}_y^3 |j, m'\rangle \\ &+ \frac{1}{4} \sum_{m'} (-1)^{m-m'} \langle j, m | \hat{S}_y^2 |j, m'\rangle^2. \end{aligned} \quad (56)$$

From error-propagation formula (53) we get

$$(\Delta\theta_{\text{mom}} \sqrt{\nu})^{-2} = F_Q + \theta^2 \left[\frac{F_Q^2}{4} - 6P_4(j, m) \right] + \mathcal{O}(\theta^3). \quad (57)$$

The measurement of parity around $\theta = 0$ is optimal for any Dicke state $|j, m\rangle$, irrespective of m . In addition, for the Twin-Fock state, with $m = 0$, estimation around $\theta = \pi/2$ is also optimal.

VII. CONCLUSIONS

Usefulness of spinor Bose-Einstein condensates for atomic interferometry is investigated experimentally nowadays [12, 17, 18, 40, 57–59], including observation of the twin Fock state [40, 57]. However, main efforts concentrate around the special case of zero magnetization. Our results show that focusing on the specific value of magnetization is very limiting.

In this paper we focused on the calculation of the Fisher information for the spin-1 Bose-Einstein condensates with thermally populated internal degrees of freedom, and show that the measurement of number of atoms in particular Zeeman component maximize its value. We introduced the concept of the effective two-mode interferometry in the three-mode system. When information about the parameter θ is contained entirely within two modes then quantum metrological properties of the three-mode state are the same as the two-mode state obtained as a trace over an unexploited mode. The same mapping can be performed for an arbitrary number n_{arb} of modes and the corresponding $\text{SU}(n_{\text{arb}})$ interferometer. In other words, the two-mode interferometry can be implemented effectively in the systems consist of atoms with higher spin provided that the interferometric transformation involves two modes only. The two-mode Fisher information is independent of θ and has Heisenberg scaling as long as the magnetization variance is smaller than 1 even for non-zero temperature. Moreover, the temperature can be a source of increasing the Fisher information as we illustrated in Section V for the coherent state arising for zero magnetization in the high magnetic field limit. Fluctuations of magnetization make the two-mode Fisher information θ dependent and, hence, introduce its optimal value for which the precision in the estimation is the best.

Our results revealed great potential of spinor condensates for quantum interferometry not only for zero magnetization but also for the macroscopic one. However, using them in practice can be of the same efficiency as coherence states because decoherence effects or detection noise prevent take advantage of their properties [60]. It is the fact for other entangled states as well. However, in the light of recent theoretical and experimental results [14, 61, 62] it is interesting to develop an alternative interferometric protocol that could diminish or even reduce

such destructive effects. This provide an interesting directions for a further work.

ACKNOWLEDGMENTS

We acknowledge discussion with K. Pawłowski. This work was supported by the Polish National Science Center Grants DEC-2015/18/E/ST2/00760.

Appendix A: Equivalent expressions for the Fisher information

According to the general definition (19), the Fisher information can be calculated also from the following expressions:

$$\begin{aligned} \mathcal{I}(\theta) &= \sum_{M,k} \frac{1}{p(\{M, k\}|\theta)} \left(\frac{\partial p(\{M, k\}|\theta)}{\partial \theta} \right)^2 \\ &= \sum_{M,k} \left(\frac{\partial \log p(\{M, k\}|\theta)}{\partial \theta} \right)^2 p(\{M, k\}|\theta) \quad (\text{A1}) \end{aligned}$$

$$= 4 \sum_{M,k} \left(\frac{\partial \sqrt{p(\{M, k\}|\theta)}}{\partial \theta} \right)^2 \quad (\text{A2})$$

$$= - \sum_{M,k} p(\{M, k\}|\theta) \frac{\partial^2}{\partial \theta^2} \log p(\{M, k\}|\theta). \quad (\text{A3})$$

Appendix B: Numerical procedure for the Fisher information calculations

The Fisher information was calculated numerically based on Eq. (A2) by rotation of density matrix written in the Fock-state representation. In this way, one consider only the representation of operators and states in a more familiar vector space. Operations such as dot product, addition and multiplication transfer into the vector space, observables are represented by square hermitian matrices, and ket states as column vectors. Eigenvectors and eigenvalues of the Hamiltonian written in the Fock state basis were used to form the density matrix 27. They were calculated with algorithms built in the MATLAB enviroment, as well as rotation of the density matrix.

Appendix C: Expressions for the error propagation formula in the case of $\langle \hat{S}_z^2 \rangle$ measurement

After some algebra one gets:

$$\frac{d}{d\theta} \langle \hat{S}_z^2(\theta) \rangle = \sin(2\theta) \left[\langle \hat{S}_x^2 \rangle - \langle \hat{S}_z^2 \rangle \right] - \cos(2\theta) \langle \{ \hat{S}_z, \hat{S}_x \} \rangle, \quad (\text{C1})$$

and

$$\begin{aligned} (\Delta \hat{S}_z^2(\theta))^2 &= (\Delta \hat{S}_z^2)^2 \cos^4 \theta + (\Delta \hat{S}_x^2)^2 \sin^4 \theta \\ &+ \cos \theta \sin^3 \theta \left[2 \langle \hat{S}_x^2 \rangle \langle \{ \hat{S}_z, \hat{S}_x \} \rangle - \langle \{ \hat{S}_x^2, \{ \hat{S}_x, \hat{S}_z \} \} \rangle \right] \\ &+ \cos^3 \theta \sin \theta \left[2 \langle \hat{S}_z^2 \rangle \langle \{ \hat{S}_z, \hat{S}_x \} \rangle - \langle \{ \hat{S}_z^2, \{ \hat{S}_x, \hat{S}_z \} \} \rangle \right] \\ &+ \cos^2 \theta \sin^2 \theta \left[\langle \{ \hat{S}_z, \hat{S}_x \}^2 \rangle - \langle \{ \hat{S}_z, \hat{S}_x \} \rangle^2 \right] \\ &+ \langle \{ \hat{S}_x^2, \hat{S}_z^2 \} \rangle - 2 \langle \hat{S}_z^2 \rangle \langle \hat{S}_x^2 \rangle, \quad (\text{C2}) \end{aligned}$$

where $\{ \cdot, \cdot \}$ denotes anti-commutator. In the case of quantum states within a fixed magnetization subspace the above formulas simplify due to

$$\langle \{ \hat{S}_z, \hat{S}_x \} \rangle = 0, \quad (\text{C3})$$

$$\langle \{ \hat{S}_x^2, \{ \hat{S}_z, \hat{S}_x \} \} \rangle = 0, \quad (\text{C4})$$

$$\langle \{ \hat{S}_z^2, \{ \hat{S}_z, \hat{S}_x \} \} \rangle = 0, \quad (\text{C5})$$

and one recovers the result of [53].

Appendix D: Wigner matrix

In the case of two-mode interferometers the function $\mathcal{D}_{k',k}^{M',M}(\hat{\Lambda}_{\mathbf{n}}, \theta)$ can be expressed in terms of the Wigner rotation matrix $d_{m,m'}^{(j)}(\theta)$ [63] for any values of θ . Therefore, when $\hat{\Lambda}_{\mathbf{n}} = \hat{\Lambda}_{\mathbf{n}}^{(A)}$ then

$$\mathcal{D}_{k',k}^{M',M}(\hat{\Lambda}_{\mathbf{n}}^{(A)}, \theta) = i^{\frac{M-M'}{2}} \delta_{k' - \frac{M'}{2}, k - \frac{M}{2}} d_{\frac{M'}{2}, \frac{M}{2}}^{(k - \frac{M}{2})}(2\theta), \quad (\text{D1})$$

and when $\hat{\Lambda}_{\mathbf{n}} = \hat{\Lambda}_{\mathbf{n}}^{2M(B)}$ one has:

$$\begin{aligned} \mathcal{D}_{k',k}^{M',M}(\hat{\Lambda}_{\mathbf{n}}^{2M(B)}, \theta) &= i^{\frac{3(k-k')}{2} - \frac{M-M'}{2}} \delta_{M' - k', M - k} \\ &d_{\frac{3k' - N - M'}{2}, \frac{3k - N - M}{2}}^{(\frac{N+M-k}{2})}(2\theta). \quad (\text{D2}) \end{aligned}$$

When the phase $\theta = 0$ for both two- and three-mode interferometry one has

$$\mathcal{D}_{k',k}^{M',M}(\hat{\Lambda}_{\mathbf{n}}, 0) = \delta_{k,k'} \delta_{M,M'} \quad (\text{D3})$$

for any $\hat{\Lambda}_{\mathbf{n}}$, and the probability distribution simply reduces to

$$p(\{M, k\}|0) = w_M \rho_{k,k}^M. \quad (\text{D4})$$

-
- [1] W. Muessel, H. Strobel, D. Linnemann, D. B. Hume, and M. K. Oberthaler, *Phys. Rev. Lett.* **113**, 103004 (2014).
- [2] M. Vengalattore, J. M. Higbie, S. R. Leslie, J. Guzman, L. E. Sadler, and D. M. Stamper-Kurn, *Phys. Rev. Lett.* **98**, 200801 (2007).
- [3] Y. Eto, H. Ikeda, H. Suzuki, S. Hasegawa, Y. Tomiyama, S. Sekine, M. Sadgrove, and T. Hirano, *Phys. Rev. A* **88**, 031602 (2013).
- [4] P. Krüger, S. Wildermuth, S. Hofferberth, L. M. Andersson, S. Groth, I. Bar-Joseph, and J. Schmiedmayer, *Journal of Physics: Conference Series* **19**, 56 (2005).
- [5] S. Wildermuth, S. Hofferberth, I. Lesanovsky, E. Haller, L. M. Andersson, S. Groth, I. Bar-Joseph, P. Krüger, and J. Schmiedmayer, *Nature* **435** (2005).
- [6] S. Wildermuth, S. Hofferberth, I. Lesanovsky, S. Groth, P. Krüger, and J. Schmiedmayer, *Appl. Phys. Lett.* **88**, 264103 (2006).
- [7] S. Aigner, L. D. Pietra, Y. Japha, O. Entin-Wohlman, T. David, R. Salem, R. Folman, and J. Schmiedmayer, *Science* **319**, 1226 (2008).
- [8] D. Kajtoch and E. Witkowska, *Phys. Rev. A* **93**, 023627 (2016).
- [9] D. Kajtoch, K. Pawłowski, and E. Witkowska, *Phys. Rev. A* **97**, 023616 (2018).
- [10] Z. Zhang and L.-M. Duan, *Phys. Rev. Lett.* **111**, 180401 (2013).
- [11] L.-N. Wu and L. You, *Phys. Rev. A* **93**, 033608 (2016).
- [12] M. Gabbrielli, L. Pezzé, and A. Smerzi, *Phys. Rev. Lett.* **115**, 163002 (2015).
- [13] S. S. Szigeti, R. J. Lewis-Swan, and S. A. Haine, *Phys. Rev. Lett.* **118**, 150401 (2017).
- [14] D. Linnemann, H. Strobel, W. Muessel, J. Schulz, R. J. Lewis-Swan, K. V. Kheruntsyan, and M. K. Oberthaler, *Phys. Rev. Lett.* **117**, 013001 (2016).
- [15] B. Lücke, M. Scherer, J. Kruse, L. Pezzé, F. Deuretzbacher, P. Hyllus, O. Topic, J. Peise, W. Ertmer, J. Arlt, L. Santos, A. Smerzi, and C. Klempt, *Science* **334**, 773 (2011).
- [16] X.-Y. Luo, Y.-Q. Zou, L.-N. Wu, Q. Liu, M.-F. Han, M. K. Tey, and L. You, *Science* **355**, 620 (2017).
- [17] C. D. Hamley, C. S. Gerving, T. M. Hoang, E. M. Bookjans, and M. S. Chapman, *Nat. Phys.* **8**, 305 (2012).
- [18] I. Kruse, K. Lange, J. Peise, B. Lücke, L. Pezzé, J. Arlt, W. Ertmer, C. Lisdat, L. Santos, A. Smerzi, and C. Klempt, *Phys. Rev. Lett.* **117**, 143004 (2016).
- [19] C. L. Degen, F. Reinhard, and P. Cappellaro, *Rev. Mod. Phys.* **89**, 035002 (2017).
- [20] L. Pezzé and A. Smerzi, in *Atom Interferometry (Proceedings of the International School of Physics)* (Societa Italiana di Fisica, 2014).
- [21] H. Strobel, W. Muessel, D. Linnemann, T. Zibold, D. B. Hume, L. A. Pezzé, Smerzi, and M. K. Oberthaler, *Science* **345**, 424 (2014).
- [22] R. Krischek, C. Schwemmer, W. Wieczorek, H. Weinfurter, P. Hyllus, L. Pezzé, and A. Smerzi, *Phys. Rev. Lett.* **107**, 080504 (2011).
- [23] C. H., *Mathematical Methods of Statistics* (Princeton, NJ: Princeton University Press) (1961).
- [24] R. A. Fisher, *Math. Proc. Camb. Philos. Soc.* **22**, 700725 (1925).
- [25] A. Holevo, *Probabilistic and Statistical Aspects of Quantum Theory* (Scuola Normale Superiore Pisa, 2011).
- [26] D. M. Stamper-Kurn and M. Ueda, *Rev. Mod. Phys.* **85**, 1191 (2013).
- [27] C. Frapolli, T. Zibold, A. Invernizzi, K. Jiménez-García, J. Dalibard, and F. Gerbier, *Phys. Rev. Lett.* **119**, 050404 (2017).
- [28] Y. Kawaguchi and M. Ueda, *Physics Reports* **520**, 253 (2012), spinor Bose–Einstein condensates.
- [29] M.-S. Chang, Q. Qin, W. Zhang, L. You, and M. S. Chapman, *Nat. Phys.* **1**, 111 (2005).
- [30] W. Zhang, D. L. Zhou, M.-S. Chang, M. S. Chapman, and L. You, *Phys. Rev. A* **72**, 013602 (2005).
- [31] H. Pu, C. K. Law, S. Raghavan, J. H. Eberly, and N. P. Bigelow, *Phys. Rev. A* **60**, 1463 (1999).
- [32] S. Yi, O. E. Mustecaplioglu, C. P. Sun, and L. You, *Phys. Rev. A* **66**, 011601 (2002).
- [33] V. Corre, *Magnetism in spin-1 Bose-Einstein condensates with antiferromagnetic interactions*, Ph.D. thesis (2014).
- [34] C. D. Hamley, *Spin-nematic squeezing in a spin-1 Bose-Einstein condensate*, Ph.D. thesis, Georgia Institute of Technology (2012).
- [35] R. Barnett, J. D. Sau, and S. Das Sarma, *Phys. Rev. A* **82**, 031602 (2010).
- [36] A. Sala, D. L. Núñez, J. Martorell, L. De Sarlo, T. Zibold, F. Gerbier, A. Polls, and B. Juliá-Díaz, *Phys. Rev. A* **94**, 043623 (2016).
- [37] L. D. Sarlo, L. Shao, V. Corre, T. Zibold, D. Jacob, J. Dalibard, and F. Gerbier, *New Journal of Physics* **15**, 113039 (2013).
- [38] Y. Huang, H.-N. Xiong, Z. Sun, and X. Wang, *Phys. Rev. A* **92**, 023622 (2015).
- [39] F. Gerbier, A. Widera, S. Fölling, O. Mandel, and I. Bloch, *Phys. Rev. A* **73**, 041602 (2006).
- [40] X.-Y. Luo, Y.-Q. Zou, L.-N. Wu, Q. Liu, M.-F. Han, M. Khoon Tey, and L. You, *Science* **355**, 620 (2017).
- [41] V. Corre, T. Zibold, C. Frapolli, L. Shao, J. Dalibard, and F. Gerbier, *EPL (Europhysics Letters)* **110**, 26001 (2015).
- [42] V. Giovannetti, S. Lloyd, and L. Maccone, *Phys. Rev. Lett.* **96**, 010401 (2006).
- [43] S. J. Seltzer, *Developments in alkali metal atomic magnetometry*, Ph.D. thesis, Princeton University (2008).
- [44] M. Sadgrove, Y. Eto, S. Sekine, H. Suzuki, and T. Hirano, *Journal of the Physical Society of Japan* **82**, 094002 (2013).
- [45] L. Pezzé and A. Smerzi, in *Atom Interferometry (Proceedings of the International School of Physics)* (Societa Italiana di Fisica, 2014).
- [46] S. L. Braunstein and C. M. Caves, *Phys. Rev. Lett.* **72**, 3439 (1994).
- [47] H. Nagaoka, in *Asymptotic theory of quantum statistical inference : selected papers*, edited by M. Hayashi (Hackensack, NJ: World Scientific, 2005) Chap. 9, pp. 113–125.
- [48] T. Wasak, A. Smerzi, L. Pezzé, and J. Chwedeńczuk, *Quantum Information Processing* **15**, 2231 (2016).
- [49] L. Pezzé and A. Smerzi, *Phys. Rev. Lett.* **110**, 163604 (2013).
- [50] L. Pezzé, A. Smerzi, M. K. Oberthaler, R. Schmied, and P. Treutlein, arXiv:1609.01609 [quant-ph] (2016).
- [51] G. Tóth and I. Apellaniz, *Journal of Physics A: Mathe-*

- matical and Theoretical **47**, 424006 (2014).
- [52] I. Apellaniz, B. Lücke, J. Peise, C. Klempt, and G. Tth, *New Journal of Physics* **17**, 083027 (2015).
- [53] Iagoba Apellaniz, Bernd Lücke, Jan Peise, Carsten Klempt and Géza Tóth, *New J. Phys.* **17** (2015).
- [54] J. J. . Bollinger, W. M. Itano, D. J. Wineland, and D. J. Heinzen, *Phys. Rev. A* **54**, R4649 (1996).
- [55] C. C. Gerry and J. Mimih, *Contemporary Physics* **51**, 497 (2010).
- [56] H. Ott, *Reports on Progress in Physics* **79**, 054401 (2016).
- [57] B. Lücke, M. Scherer, J. Kruse, L. Pezzé, F. Deuretzbacher, P. Hyllus, O. Topic, J. Peise, W. Ertmer, J. Arlt, L. Santos, A. Smerzi, and C. Klempt, *Science* **334**, 773 (2011).
- [58] T. M. Hoang, H. M. Bharath, M. J. Boguslawski, M. Anquez, B. A. Robbins, and M. S. Chapman, *PNAS* **113**, 9475 (2016).
- [59] J. Peise, I. Kruse, K. Lange, B. Lücke, L. Pezzé, J. Arlt, W. Ertmer, K. Hammerer, L. Santos, A. Smerzi, and C. Klempt, *Nature Communications* **6**, 8984 (2015).
- [60] R. Demkowicz-Dobrzański, J. Czajkowski, and P. Sekatski, *Phys. Rev. X* **7**, 041009 (2017).
- [61] E. Davis, G. Bentsen, and M. Schleier-Smith, *Phys. Rev. Lett.* **116**, 053601 (2016).
- [62] S. P. Nolan, S. S. Szigeti, and S. A. Haine, *Phys. Rev. Lett.* **119**, 193601 (2017).
- [63] L. C. Biedenharn and J. D. Louck, *Angular Momentum in Quantum Physics: Theory and Applications* (Cambridge University Press, Cambridge) (1984).